Chapter

Abrasive Wear Performance of Fe_2B Layers Applied on Steel Substrates

Armando Irvin Martínez Pérez, Edgar Ernesto Vera Cárdenas, Manuel Vite Torres, José Luis Bernal Ponce, Karina Alemán Ayala and Marisa Moreno Rios

Abstract

The resistance of dry abrasive wear in Fe_2B layer deposited on AISI D2 and 1040 steel substrates, using the powder-pack boriding process, was evaluated. The boriding process was carried out at temperatures of 1220 and 1320 K for a time of 8 h. A Rockwell hardness tester was used to assess the Daimler-Benz adhesion test. The abrasive wear tests were carried out in dry conditions according to the ASTM G65 test standard. The test parameters used were a sand flow of 400 g/min, a nominal rubber wheel constant rotation of 200 rpm, a load of 122 N, and a sliding distance of 716.28 m. The type of abrasive used was steel round grit with a grain size of 260 μm and a hardness of 1100 HV. The total time for each test was 30 min, removing the specimens every 5 min to determine the amount of mass loss using an analytical balance (sensitivity of 0.0001 g). The average value of volume loss and wear rates is reported. Optical microscopy and SEM were carried out in order to identify the wear mechanisms. The wear mechanisms presented in this study were two-body abrasive wear, pitting action, and plastic deformation.

Keywords: dry abrasive wear, Fe_2B layer, steel substrates, boriding, wear mechanisms

1. Introduction

Abrasive wear occurs when a hard particle slides on a surface, causing loss of material. This type of wear depends on factors such as hardness, roughness, and particle geometry [1–4].

Different coatings are used as anti-abrasive wear materials. Some of them are as follows: ceramics coatings, such as, Al_2O_3/TiO_2, $SiO_2/TiO_2/Cr_2O_3$, SiC, B_4C, ZrO_2, CaO, CrN/AlCrN, CrN/BCN, SiO_2, WC, and TiC [5, 6]; polymer coatings [7, 8]; and DLC coatings [9, 10].

On the other hand, some works have been developed using boron coatings as anti-wear material. Boronizing is a thermo-diffusion process in which boron atoms, due to their small diameter and high mobility at elevated temperatures, diffuse into a metal surface and form intermetallic compounds with atoms of base metal [11]. Abrasive wear tests were carried out using boronizing on SAE 1010, 1040, D2, and 304 steels [12]. It was seen that boronizing improved the wear strengths

considerably. The best abrasive wear strengths were obtained in boronizing for 8 h at 900°C for SAE 1010 and SAE 1040 steels, 4 h at 900°C for D2 steel, and 6 h at 900°C for 304 steel. In another work [13], abrasive wear resistance of boride layers on Fe-15Cr alloy was studied. It was found that the dry abrasive wear resistance of borided alloy samples was around 45 times greater than that of non-borided ones. In another study [14], the micro-abrasive wear of boride layers on AISI D2 tool steel was investigated. Some results indicated that wear resistance of the borided samples was superior to the hardened, uncoated AISI D2 steel. According to literature [15], wear resistance of boronized steels in abrasive wear conditions depends on the phase composition and hardness of the layer and its stress state, but the hardness of abrasive particles also has a significant importance on the wear speed.

The objective of this work was to evaluate the resistance of dry abrasive wear in Fe_2B layer deposited on AISI D2 and 1040 steel substrates without a previous heat treatment (hardened and tempered) using the powder-pack boriding process. The substrate materials were selected in order to compare the wear abrasion behavior of a plain carbon (1040) versus a high-carbon, high-chromium steel (D2). AISI 1040 steel is frequently cold drawn to specified physical properties for use without heat treatment for some practical applications such as cylinder head studs. AISI D2 tool steel has desirable properties such as abrasion resistance, high hardness, and no deforming characteristics, and is used in lamination and stamping dies, shear blades, master tools, etc. The wear resistance of D2 tool steel is approximately eight times that of plain carbon steels, so also was of interest to know if this great difference in wear behavior could increase or decrease in borided conditions.

2. Experimental work

2.1 Test specimens

The specimens had a rectangular shape with dimensions of 50 × 25 mm and 10 mm in thickness. The chemical composition of the AISI D2 and 1040 steels is shown in **Table 1** [16, 17].

The boriding process used in the specimens of AISI D2 and 1040 steel substrates was the same as reported in a previous work [18]. The only difference is that for this work, two boriding temperatures were employed (1220 and 1320 K).

It is important to mention that, based on the Fe-B phase diagram and the high iron content of the AISI D2 and 1040 steels [19], in addition to the diffusion of boron at high temperatures (1220 and 1320 K) and the treatment time of 8 h, the formation of a Fe_2B monolayer is ensured under the conditions of the boriding process proposed in this work. Because the Fe-B phase is formed on the surface of the sample, which generates the Fe-B/Fe interface between the Fe-B phase and the steel, this allows the gradual formation of the Fe_2B phase that grows when the thickness of the boride is increased and at the same time the Fe-B phase decreases. At the

Steel	Composition								
	C	Mn	Si	Cr	Mo	V	S	P	Fe
AISI D2	1.55	0.35	0.35	11.8	0.85	0.85	0.03	0.03	84.22
AISI 1040	0.38	0.6	0.1	0	0	0	0.02	0.02	98.87

Table 1.
Chemical composition of specimens (wt.%).

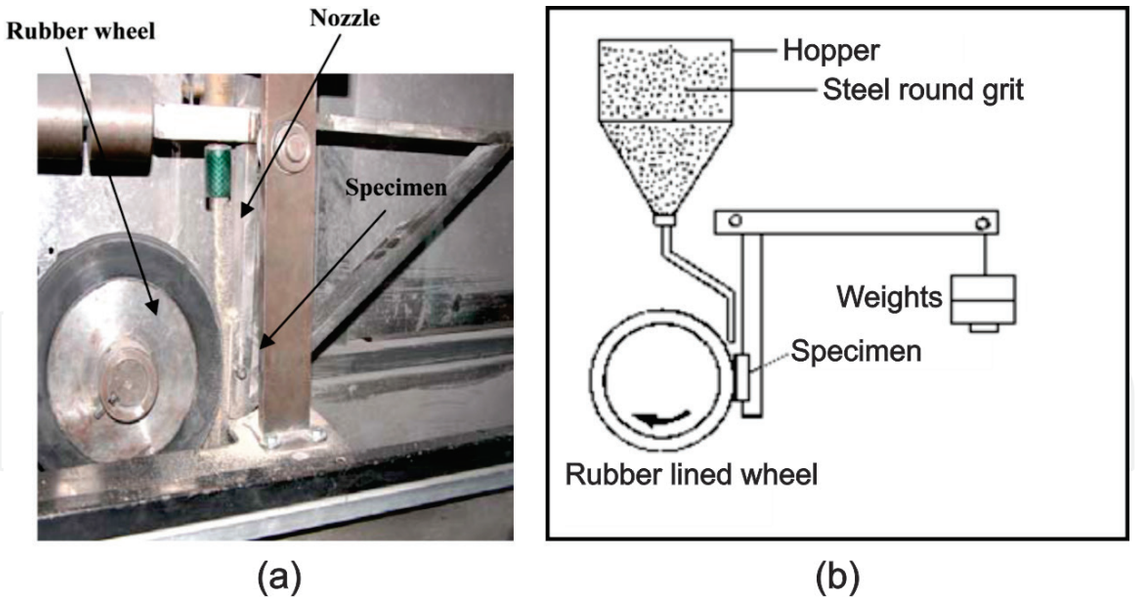

Figure 1.
(a) Experimental setup and (b) schematic diagram of the apparatus.

end of the 8 h, corresponding to the treatment time, the Fe-B phase was consumed completely, and so the only phase present (Fe_2B) stops growing [20].

2.2 Test procedure

The tests were performed according to the ASTM G65 test standard [21]. **Figure 1** shows the experimental rig and a simplified schematic diagram of the dry/sand rubber wheel apparatus used in this research work [22].

The test parameters used were a sand flow of 400 g/min, a nominal rubber wheel constant rotation of 200 rpm, a load of 122 N, and a total sliding distance of 716.28 m, using a 228.6 mm diameter wheel rotating. The wheel consists of a steel disk with an outer layer of neoprene rubber tire molded to its periphery with hardness A60. As the rubber wheel reduces in diameter, the number of wheel revolutions was adjusted to equal the sliding distance of the new wheel. The type of abrasive used was steel round grit with a grain size of 260 μm and a hardness of 1100 HV. The total time for each test was 30 min, removing the specimens every 5 min to determine the amount of mass loss using an analytical balance (sensitivity of 0.0001 g). Before the overall tests were performed, the specimens were cleaned by washing in ethanol in an ultrasonic bath (Fisherbrand 11020).

The average value of volume loss (V), wear rates (Q), and wear coefficients (k) are reported. Optical microscopy and SEM were carried out on the damaged surfaces in order to identify the wear mechanisms. Additionally, the profiles of the wear scars are presented using a Mitutoyo Surftest Profilometer.

3. Results and discussion

3.1 Fe_2B layer hardness

A load of 100 g was used to evaluate the hardness of Fe_2B layers with a Vickers indenter. The variation of the hardness, depending on the depth of layers, is shown in **Figure 2**. Also, the roughness of specimens was obtained with a Mitutoyo Surftest Profilometer, see **Table 2**.

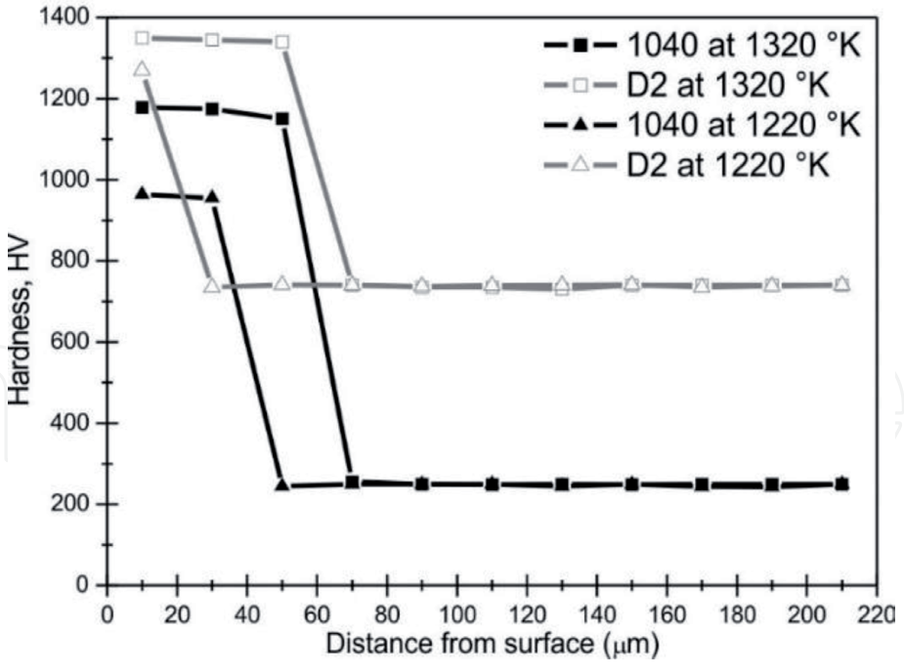

Figure 2.
Variation of hardness.

Boriding temperature (K)	Borided steel	Vickers hardness (HV)	Roughness (Ra) (μm)
1220	AISI D2	1270.7	0.86
	AISI 1040	964.4	1.14
1320	AISI D2	1354.5	0.22
	AISI 1040	1179.5	0.35

Table 2.
Properties of the specimens.

3.2 SEM, X-ray diffraction, and EDS

Figure 3 shows the cross-sectional view of SEM micrographs. A zigzag teeth shape is observed in both steels. This columnar shape comes from the direction in which diffusion is preferred, and the boride is of stronger (002) texture [23]. The presence of this typical morphology for good adhesion between coating and substrate is necessary.

The boriding is a diffusive process highly anisotropic [24]. In **Figure 3**, it was observed that the boride on the surface of AISI D2 steel presents a columnar morphology; in the case of boride formed on the surface of AISI 1040 mold steel is observed a dense structure due to alloying elements it has. Depending on the conditions of processing time, temperature, and chemical composition of substrates, the depth obtained of the boride layer was an interval of 10–60 μm (**Figure 2**). It was observed that the depth of borides formed on AISI D2 is more homogeneous than that of AISI 1040.

The results of X-ray diffraction studies are presented in **Figure 4**. The XRD analysis shows well-defined peaks at 42.67 and 45.11° confirming Fe_2B phase. Also, the presence of chromium boride (CrB) phase in the borided AISI D2 steel was determined. This is due to the significant presence of chromium in AISI D2 steel as an alloying element [25, 26]; apparently, during powder-pack boriding, it reacted with boron atoms and formed a little intermediate phase of CrB.

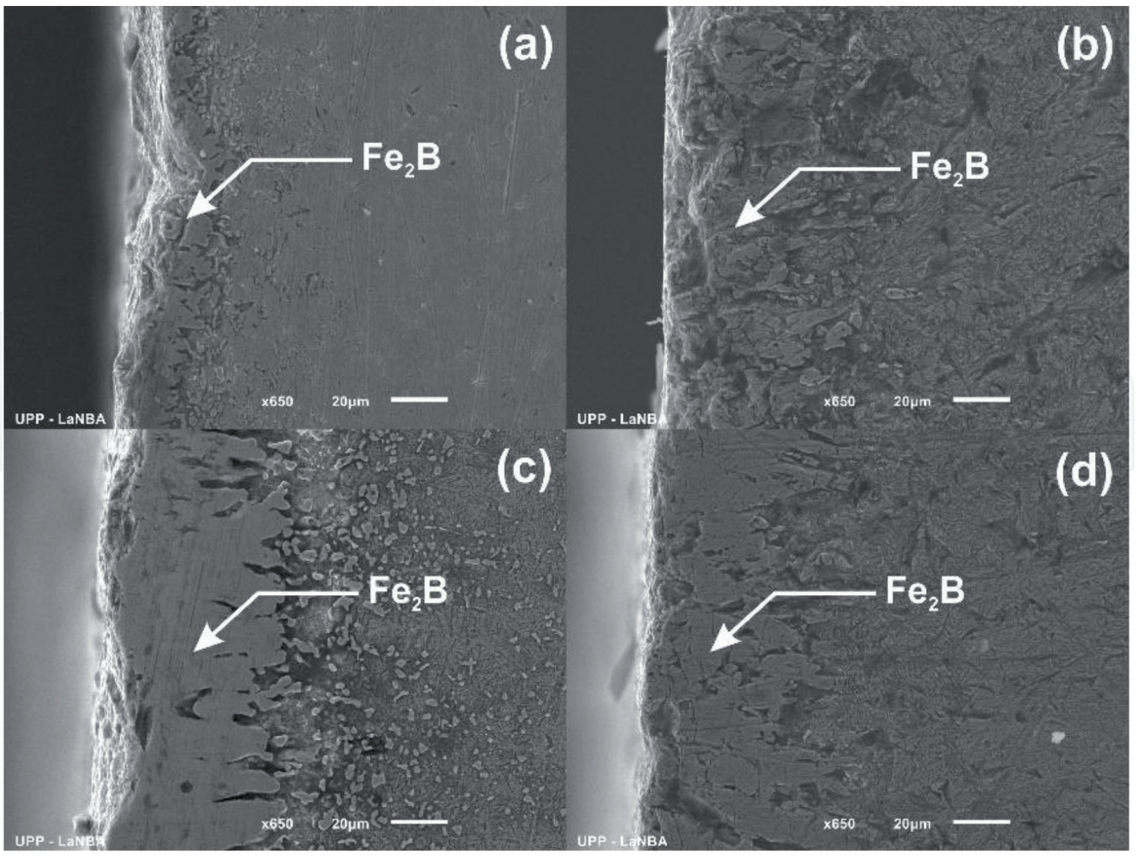

Figure 3.
SEM cross-sectional micrograph, and XRD of borided samples: (a) AISI D2 at 1220 K, (b) AISI 1040 at 1220 K, (c) AISI D2 at 1320 K and (d) AISI 1040 at 1320 K.

The EDS analysis obtained by SEM, for the borided steels, is shown in **Figure 5a–d**. The presence of borides formed on the surfaces of the steels was confirmed considering the presence of boron and iron.

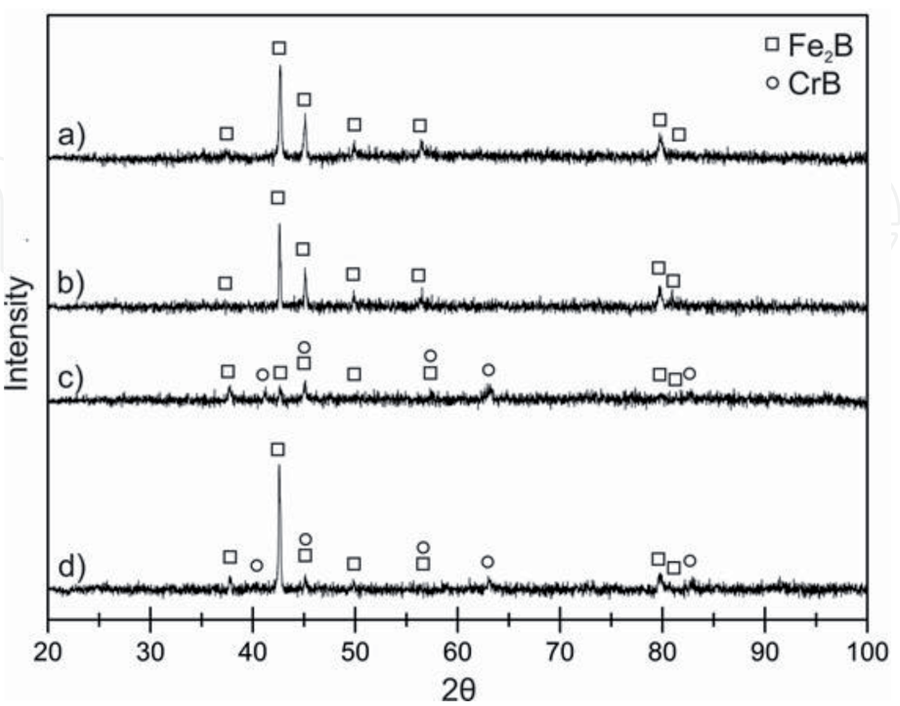

Figure 4.
Diffraction patterns of borided specimens: (a) AISI 1040 at 1220 K, (b) AISI 1040 at 1320 K, (c) AISI D2 at 1220 K, and (d) AISI D2 at 1320 K.

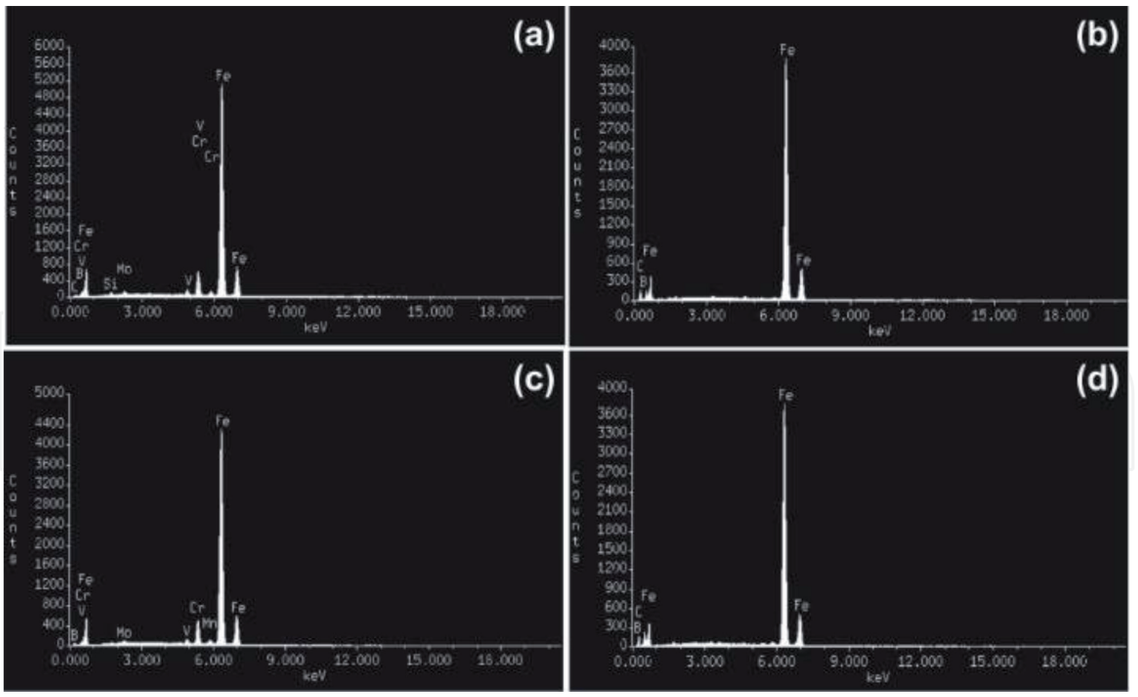

Figure 5.
EDS spectrum of borided samples. (a) AISI D2 at 1220 K, (b) AISI 1040 at 1220 K, (c) AISI D2 at 1320 K, and (d) AISI 1040 at 1320 K.

3.3 Fe_2B layer adhesion test

A Cientec Rockwell hardness tester model 200HR-150 was used to assess the Daimler-Benz adhesion tests [27]. **Figure 6** shows the indentations on the surfaces. For the AISI D2 steel, some small cracks and no visible delamination are observed (**Figure 6a** and **c**), and the adhesion strength quality is related to HF1 map [28]. In the case of AISI 1040 steel (**Figure 6b** and **d**), microcracks and small delamination are observed, and the adhesion category belongs to the HF4 level.

3.4 Wear profile

The abrasion tests carried out caused wear damage on surfaces. The wear profiles were measured using a Mitutoyo Surftest profilometer and are shown in **Figure 7**. The results are compatible with the volume loss (**Figure 8**), where 1040 steel borided at 1220 K has the greatest wear volume and the D2 steels at 1320 K had the minor wear.

3.5 Volume loss

The volume loss was obtained for all the borided and unborided steel substrates. These data were calculated using Eq. (1). The mass loss was obtained weighing the specimens before and after the test. The graph of the **Figure 8** shows that the AISI D2 steel borided at 1320 K exhibited a higher wear resistance compared to the other specimens. The results also show the great difference in volume loss between borided and unborided steels. The reason that the D2 steel had a greater wear resistance is due most likely to the mechanical properties conferred by a high content of C and Cr, which is higher than in the 1040 steel (see **Table 1**). According to **Figure 8**, the abrasion wear resistance of borided D2 tool steel is approximately 16 times greater than borided 1040 plain carbon steel. This could justify the use of this tool steel for abrasion wear applications when it is borided to the conditions used in this work,

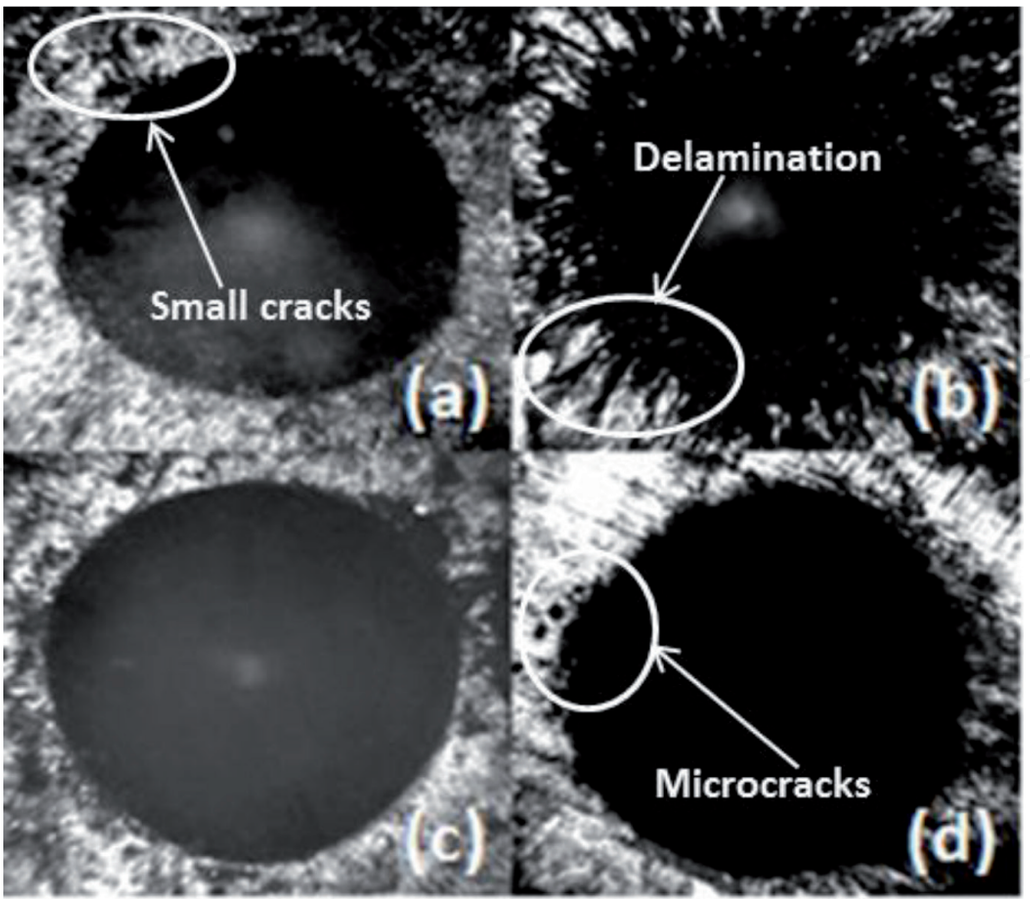

Figure 6.
Indentations on surfaces. (a) AISI D2 borided at 1220 K, (b) AISI 1040 borided at 1220 K, (c) AISI D2 borided at 1320 K, and (d) AISI 1040 borided at 1320 K.

without a previous heat treatment, as usual. These results also indicate that its core strength was not affected due to high temperatures of powder-pack boriding treatment.

$$\text{Volume loss } (\text{mm}^3) = \left(\text{Mass loss } (\text{g})/\text{density } \left(\text{g}/\text{cm}^3\right)\right) \times 1000 \qquad (1)$$

3.6 Wear rates (Q) and wear coefficients (k)

The wear rates were obtained from Eq. (2).

$$Q = V/d. \qquad (2)$$

where Q = wear rate (mm^3/m), V = volume loss (mm^3), and d = sliding distance (m).

Figure 9 shows the wear rates obtained every 716 m of the borided and unborided D2 and 1040 steels. AISI D2 borided steels at 1320 and 1220 K had the best performance against the dry abrasive wear conditions. It was due to its good mechanical properties and chemical composition. Additionally, the adhesion tests on this steel showed an excellent performance. On the other hand, the 1040 steel borided at 1320 K had a good behavior, almost similar to the D2 steel. For the AISI 1040 steels borided at 1220 K, an abnormal value was observed at a sliding distance of 716 m, where the wear rate had a great increase. This performance was mainly due to the running in period of the test.

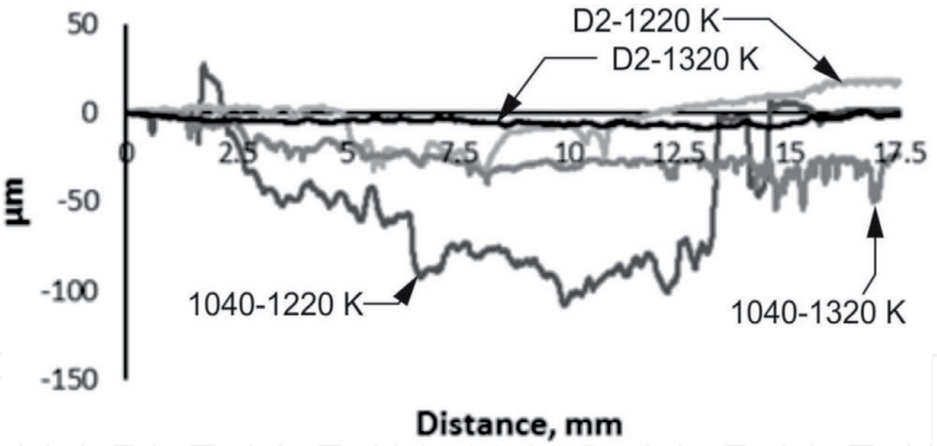

Figure 7.
Roughness profiles of wear scars.

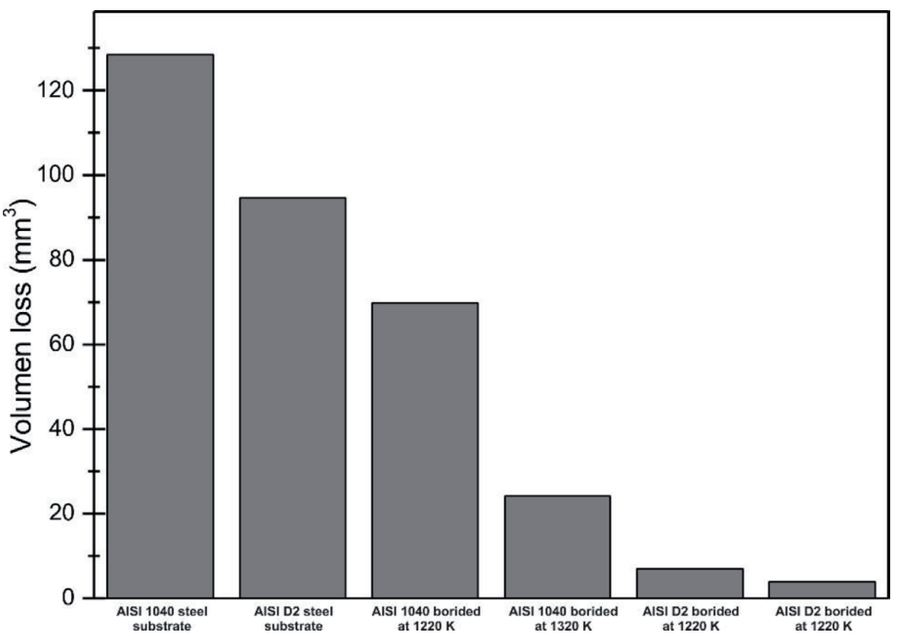

Figure 8.
Volume loss of borided and unborided steels.

3.7 Wear mechanisms

Figure 10a–f shows the wear on the surface of the unborided and borided specimens. In both steels, as expected, the wear damage was more severe on the unborided specimens (**Figure 10a** and **b**). In the case of the borided steels, AISI 1040 at 1220 K (**Figure 10c**) showed the greater damage and the AISI D2 borided at 1320 K (**Figure 10d**) showed the lower damage. This was in accordance to the results of the wear profiles showed in **Figure 7** and wear rates showed in **Figure 9**. In the case of borided steels, the main wear mechanism observed in the wear scars was the two-body abrasive wear due to the presence of parallel lines to the sliding direction. These parallel lines were produced by wear debris acting as indenters causing, in some cases, depth grooves.

Figure 11a–d shows the SEM micrographs of the wear damage of the borided steels. In the case of AISI 1040 steel borided at 1220 K (**Figure 11a**), wear debris was observed, which was derived from the three-body abrasion situation, where hard particles were trapped between the two sliding surfaces. Also, severe pitting action was observed, caused by the particles of material and abrasive particles. Finally,

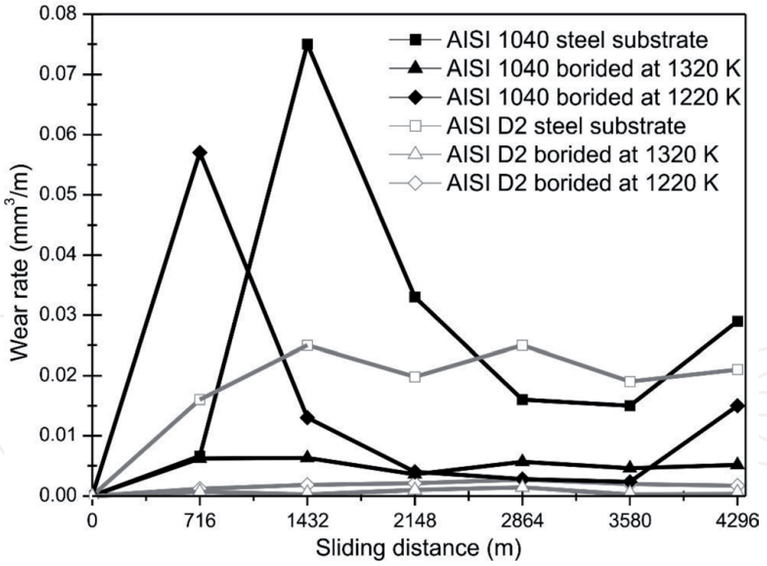

Figure 9.
Wear rate of borided and unborided steels.

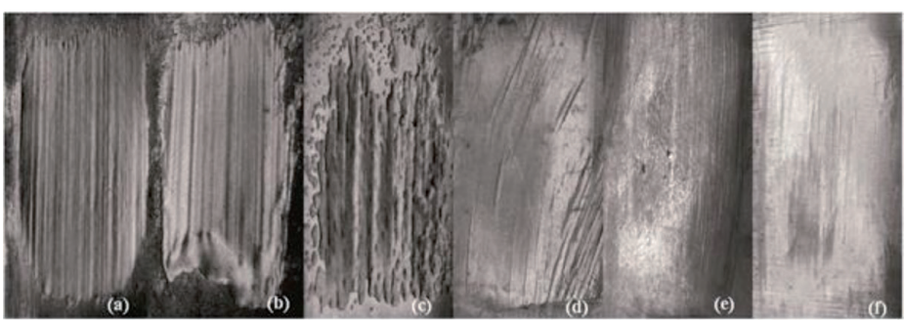

Figure 10.
(a) 1040 steel substrate, (b) D2 steel substrate (c) 1040 borided—1220 K, (d) D2 borided—1220 K, (e) 1040 borided—1320 K, and (f) D2 borided—1320 K.

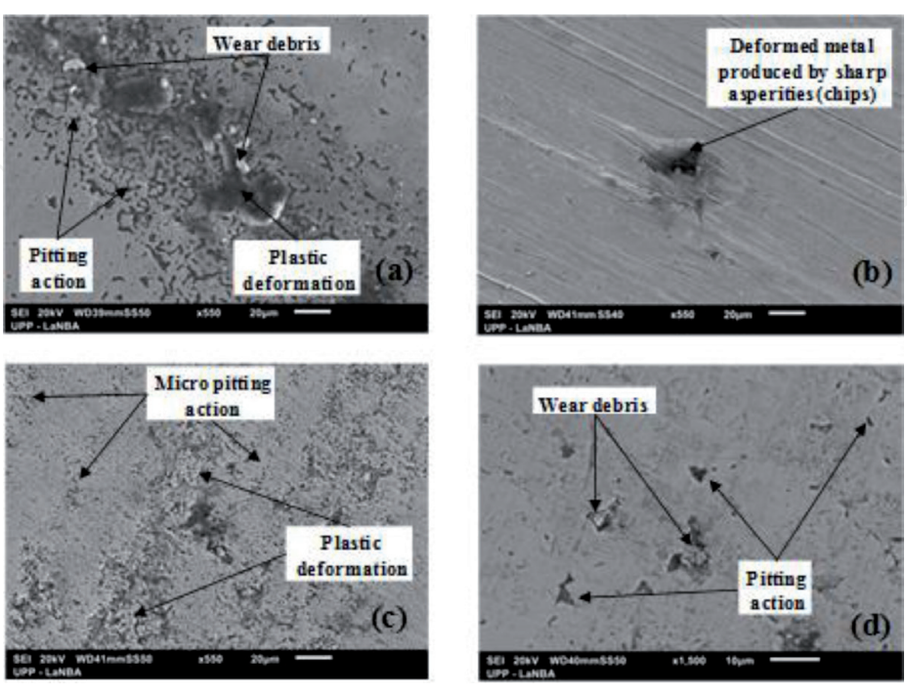

Figure 11.
SEM micrographs of wear scars. (a) AISI 1040 at 1220 K, (b) AISI D2 at 1220 K, (c) AISI 1040 at 1320 K, and (d) AISI D2 at 1320 K.

plastic deformation occurred due mainly to the sliding action. **Figure 11b** (AISI D2 steel at 1220 K) shows a typical effect of abrasive wear, where sharp asperities plowed the surface, causing permanent deformation. This plowing action produced a groove in the softer material. Also, parallel lines were observed caused by wear debris probably inlaid in the rubber wheel. In the case of AISI 1040 steel borided at 1320 K (**Figure 11c**), severe micropitting action and plastic deformation were observed. Finally, in the case of the AISI D2 steel at 1320 K, wear debris and pitting action were observed, but to a lesser degree. This matches with the results of wear rates obtained and indicated in **Figure 9**.

4. Conclusions

1. The formation of a Fe_2B monolayer is ensured under the conditions of the process of boron powder-pack proposed in this work. The Fe-B phase is formed on the surface of the sample, which generated the Fe-B/Fe interface between the Fe-B phase and the steel, which allowed the gradual formation of the Fe_2B phase that grows when the thickness of the boride is increased and at the same time the Fe-B phase decreases.

2. The Rockwell-C adhesion tests showed that for the AISI D2 steel, the adhesion strength quality, of Fe_2B layers, is related to HF1 map, showing some small microcraks and the AISI 1040 steel fits to HF4 category, where microcracks and some delamination was observed.

3. AISI D2 steel specimens borided at 1320 K showed a higher wear resistance, in accordance to the wear rates and wear coefficients results. It was due to its good mechanical properties and chemical composition. Additionally, the adhesion tests on this steel showed an excellent performance.

4. The wear mechanisms presented in this study were as follows: two-body abrasive wear, which was due to the presence of parallel lines to the sliding direction; pitting action, which was caused by the particles of the material and abrasive particles; and plastic deformation, which occurred due mainly to the sliding action.

Author details

Armando Irvin Martínez Pérez[1], Edgar Ernesto Vera Cárdenas[2*], Manuel Vite Torres[3], José Luis Bernal Ponce[4], Karina Alemán Ayala[5] and Marisa Moreno Rios[2]

1 Polytechnic University of Pachuca, Zempoala, Hidalgo, Mexico

2 National Technology of Mexico/Technological Institute of Pachuca, Pachuca, Hidalgo, Mexico

3 National Polytechnic Institute, ESIME Zacatenco, Mexico City, Mexico

4 National Technology of Mexico/Technological Institute of Orizaba, Orizaba, Veracruz, Mexico

5 Autonomous University of the State of Hidalgo, Mineral de la Reforma, Hidalgo, Mexico

*Address all correspondence to: eevc2000@hotmail.com

References

[1] Rabinowicz E. Friction and Wear of Materials. New York, USA: Wiley; 1965

[2] Bhushan B. Introduction to Tribology. New York, USA: Wiley; 2002

[3] Khruschov MM. Principles of abrasive wear. Wear. 1974;**28**:69-88

[4] ASTM G40-17. Standard Terminology Relating to Wear and Erosion. 2017

[5] Mo JL, Zhu MH. Sliding tribological behaviors of PVD CrN and AlCrN coatings against Si_3N_4 ceramic and pure titanium. Wear. 2009;**267**: 874-881

[6] Czerwinski F. Thermochemical Treatment of Metals. Croatia: Intech; 2012

[7] Zhu F, Wang J, Li S, Zhang J. Preparation and characterization of anodic films on AZ31B Mg alloy formed in the silicate electrolytes with ethylene glycol oligomers as additive. Applied Surface Science. 2012;**258**:8985-8990

[8] Brzeziński S, Kowalczyk D, Borak B, Jasiorski M. Applying the sol–gel method to the deposition of nanocoats on textiles to improve their abrasion resistance. Journal of Applied Polymer Science. 2012;**125**:3058-3067

[9] Corbella C, Rubio-Roy M, Bertran E, Polo MC, Pascual E, Andújar JL. Low friction and protective diamond-like carbon coatings deposited by asymmetric bipolar pulsed plasma. Diamond and Related Materials. 2009;**18**:1035-1038

[10] He F, Wong PL, Zhou X. Wear properties of DLC-coated steel rollers running with highly contaminated lubrication. Tribology International. 2010;**43**:990-996

[11] Milinović A, Krumes D, Marković R. An investigation of boride layers growth kinetics on carbon steels. Tehnički vjesnik. 2012;**19**:27-31

[12] Atik E, Yunker U, Meric C. The effects of conventional heat treatment and boronizing on abrasive wear and corrosion of SAE 1010, SAE 1040, D2 and 304 steels. Tribology International. 2003;**36**:155-161

[13] Dybkov VI, Goncharuk LV, Khoruzha VG, Samelyuk AV, Sidorko VR. Growth kinetics and abrasive wear resistance of boride layers on Fe–15Cr alloy. Materials Science and Technology. 2011;**27**:1502-1512

[14] Oliveira CK, Lombardi AN, Totten GE, Casteletti LC. Micro-abrasive wear of boride layers on AISI D2 tool steel produced by the thermoreactive process. International Journal of Microstructure and Materials Properties. 2008;**3**:241-253

[15] Krukovich MG, Prusakov BA, Sizov IG. Plasticity of Boronized Layers. Russia: Springer; 2016. pp. 250-253

[16] ASTM A681-08. Standard Specification for Tool Steels Alloy; 2015 (Reapproved)

[17] ASTM A510-03. Standard Specification for General Requirements for Wire Rods and Coarse Round Wire, Carbon Steel. 2003

[18] Vera Cardenas E, Lewis R, Martinez Perez A, Bernal Ponce J, Perez Pinal F, Ortiz Dominguez M, et al. Characterization and wear performance of boride phases over tool steel substrates. Advances in Mechanical Engineering. 2016;**8**(2):1-10

[19] Repovský P, Homolová V, Čiripová L, Kroupa A, Zemanová A. Experimental study and thermodynamic modelling of the

B-Fe-Mn ternary system. CALPHAD: Computer Coupling of Phase Diagrams and Thermochemistry. 2016;**55**:252-259

[20] Yu LG, Chen XJ, Khor KA, Sundararajan G. Fe-B/Fe_2B phase transformation during SPS pack-boriding: Boride layer growth kinetics. Acta Materialia. 2005;**53**:2361-2368

[21] ASTM G65-04. Standard Test Method for Measuring Abrasion Using the Dry Sand/Rubber Wheel Apparatus. 2010

[22] Vite Torres M, Moreno Rios M, Gallardo Hernandez E, Laguna Camacho J. A study of the abrasive resistance of sputtered CrN coatings deposited on AISI 316 and AISI H13 steel substrates using steel particles. Wear. 2011;**271**:1273-1279

[23] Martini C, Palombarini G, Carbucicchio M. Mechanism of thermochemical growth of iron borides on iron. Journal of Materials Science. 2004;**39**:933-937

[24] Uslu I, Comert H, Ipek M, Celebi FG, Ozdemir O, Bindal C. A comparison of borides formed on AISI 1040 and AISI P20 steels. Materials and Design. 2007;**28**:1819-1826

[25] Aronsson B, Aselius J. The effect of boron on the formation of α-FeCr at 700°C. Acta Chemical Scandinavica. 1958;**12**:1476-1480

[26] Nedfors N, Primetzhofer D, Wang L, Lu J, Hultman L, Jansson U. Characterization of magnetron sputtered Cr–B and Cr–B–C thin films for electrical contact applications. Surface and Coatings Technology. 2015;**266**:167-176

[27] Taktak S, Tasgetiren S. Identification of delamination failure of boride layer on common Cr-based steels. Journal of Materials Engineering and Performance. 2006;**15**:570-573

[28] Verein Deutscher Ingenieure Normen VDI 3198. Düsseldorf: VDI-Verlag (Coating (CVD, PVD) of cold forging tools); 1991. pp. 1-8